Methanol masers and millimetre lines : a common origin in protostellar envelopes

Torstensson, K.J.E.

CHAPTER 5

Dynamics of 6.7 GHz methanol masers in high-mass star-forming regions

II. Sources with confined thermal CH_3OH emission

Abstract

The 6.7 GHz CH_3OH maser serves as a signpost of high-mass star formation. Moreover, a recent VLBI study has shown that in 30% of the sources the CH_3OH masers occur in ring-like structures on scales of a few hundreds of AU and with velocity fields indicative of infall or outflow. On larger physical scales, in a sample of twelve high-mass star-forming regions, seven have been found to have confined (<0.4 pc) thermal CH_3OH emission thus making them suitable for a study of the relation of the thermal CH_3OH emission and the CH_3OH maser emission. To test the hypothesis that there is a common origin of the 6.7 GHz CH_3OH maser emission and the thermal CH_3OH emission, we have compared the maser emission in seven sources with the position and orientation of that of the thermal emission. The European VLBI Network has been used to map at high resolution the 6.7 GHz methanol maser emission in a sample of five sources that all have compact thermal CH_3OH emission. Phase referencing allows for determining the position to milli-arcsec accuracy. A further two sources with compact thermal CH_3OH emission that recently have been mapped with the EVN have been included. Three (AFGL5142, G73.06, and G78.12) of the five sources observed by us with the EVN were successfully mapped and the 6.7 GHz CH_3OH maser emission has a physical extent between 330 and 1700 AU. For the two sources (L1206 and G40.62) that we were unable to map CH_3OH maser data from the literature have been used, this is also the case for the last two sources (G23.207 and G23.389) that were recently observed with the EVN. In all seven sources in this study the CH_3OH maser emission arises close (<0.05 pc) to the centre of the thermal CH_3OH emission. Further, in at least three of the seven sources the major axis of the CH_3OH maser emission is roughly perpendicular to the velocity gradient seen in the thermal CH_3OH emission. The position of the CH_3OH maser emission close to the centre of

the thermal CH_3OH distribution is in accordance with a common origin of the gas phase CH_3OH in these sources. Further, in several sources the CH_3OH masers seem to delineate or be part of a disk or torus in the equatorial region of the YSO with major axes orthogonal to that of the thermal CH_3OH velocity field and we suggest that the thermal CH_3OH is entrained in a bipolar outflow. The high sensitivity and high resolution capabilities of new instruments such as ALMA will allow us to probe these regions in an unprecedented manner.

5.1 Introduction

Since their discovery twenty years ago (Menten 1991a) the 6.7 GHz CH_3OH masers have been shown to be associated with the earliest stages of high-mass star formation. To date, there are >800 known CH_3OH maser sites (Green et al. 2009). A study of the radio continuum emission towards 233 CH_3OH maser sites shows that only ~25% of the CH_3OH masers are associated with HII regions (Walsh et al. 1998). In contrast, submillimetre continuum from warm dust has been detected towards more than 95% of the 6.7 GHz CH_3OH masers (Hill et al. 2005). Recent studies suggest that the CH_3OH maser turns on before the H_2O and OH masers that are sometimes associated with the same sources (Breen et al. 2010). The water masers typically span a larger velocity range than the methanol masers and it is therefore likely that they occur in different physical structures (Bartkiewicz et al. 2011). The sources studied with high resolution VLBI techniques show that the CH_3OH maser distributions typically have extents between 100 and 2000 AU with different morphologies and have been classified as: simple, linear, complex, and disks (Norris et al. 1998, Phillips et al. 1998, Minier et al. 2002, Pestalozzi et al. 2004, Bartkiewicz et al. 2009). However, some sources have been found to be embedded in larger structures seen at shorter baselines (Pandian et al. 2011).

A recent VLBI study showed that 30% (9 of 31) of the sources selected from a blind survey of 6.7 GHz CH_3OH masers had an elliptical morphology (Bartkiewicz et al. 2009). The morphology suggests that the masers occur in a ring-like structure and that the exciting source(s) are in the centre of the ring as in the spectacular Ring source (G23.657−00.127) (Bartkiewicz et al. 2005a) and Cepheus A (Cep A) HW2 (Chapter 2). Moreover, the lack of cm continuum emission in the elliptical sources compared to the rest of the sample suggests an earlier evolutionary stage prior to any detectable free-free emission. The velocity field of the maser spots indicates that both radial and rotational velocities are important, which together with the ellipse location suggest that the maser emission occurs in a "torus" in the equatorial region of the protostar. However, with the maser observations alone it is not possible to determine the orientation of the ring and consequently not possible to distinguish outflow motions from those of infall.

Furthermore, the CH_3OH masers have recently been used to probe the magnetic field on similarly small scales (mas) and in at least two sources the magnetic field appears to be funnelling the infalling gas through a circumstellar torus around the protostellar object towards the accretion disk (Vlemmings et al. 2010, Surcis et al. 2011).

The H_2O masers and radio continuum seen on size scales similar to the CH_3OH maser emission appear to be associated with disk winds, thermal jets, and outflows (Torrelles et al. 2011). On parsec scales, molecular outflows are common signatures of these small scale processes. However, source multiplicity, with overlapping outflows and precession of the outflows, often complicates the picture and it can be difficult to trace the larger scale outflows back to a particular protostar and determine its orientation.

Recent studies have shown that in AFGL 5142 the velocity field of the CH_3OH masers can be described by a radial infall whereas the H_2O masers associated with the source seem to trace the disk wind (Goddi et al. 2007). In the case of G78.12 (IRAS 20126+4104) the CH_3OH maser emission seems to arise in two distinct regions, one

Table 5.1: Coordinates of the science targets phase centres and calibrators observed with the EVN.

Source	Coordinates (J2000)		θ	Cal.
	RA (h m s)	Dec (°′″)	°	
AFGL 5142	05 30 48.0	+33 47 55		A
J0518+3306	05 18 05.1425	+33 06 13.365	2.7	
G73.06	20 08 09.8	+35 59 20		B,C
J2016+3600	20 16 45.6188	+36 00 33.374	1.7	
G78.12	20 14 26.1	+41 13 31		B,C
J2007+4029	20 07 44.9449	+40 29 48.604	1.5	
G40.62-0.14	19 06 00.0	+06:47:22		B,C
J1912+0518	19 12 54.2577	05 18 00.421	2.3	
L1206	22 28 51.5000	+64 13 42.000		A,B,C
J2232+6249	22 32 22.8655	+62 49 36.436	1.5	
J2208+6519	22 08 03.1103	+65 19 38.791	2.5	
DA193	05 55 30.8056	+39 48 49.165		A
3C345	16 42 58.8100	+39 48 36.994		B
3C454.3	22 53 57.7479	+16 08 53.561		C

Notes: θ is the angular separation between maser and phase calibrator. A, B & C designates the amplitude and bandpass calibrators used for each source respectively.

group of maser spots seems to trace the disk and a second group appears to be associated with the disk wind interface. Also in this source the H_2O masers are associated with outflow and appear to trace a conical jet (Moscadelli et al. 2005, 2011).

In Chapter 4 we mapped the distribution and kinematics of the thermal CH_3OH emission in a sample of high-mass star-forming regions. Based on those results we classified seven of the twelve observed sources as having confined (< 0.4 pc) thermal CH_3OH emission. The aim of this chapter is to compare how the CH_3OH maser emission in these seven sources is related to the thermal CH_3OH emission and other outflow tracers. We present EVN observations of the 6.7 GHz CH_3OH maser in three (AFGL 5142, G73.06, and G78.12) of these seven sources. Of the four remaining sources, two (G23.207 and G23.389) have been classified as having elliptical maser distributions (Bartkiewicz et al. 2009), and also for the remaining two sources (L1206 and G40.62) maser data from the literature have been used.

5.2 Observations and data reduction

The EVN observations were performed in Nov 2004 as part of a larger project EL032. The telescopes participating in the experiment were Effelsberg, Westerbork, Medicina, Onsala, Toruń, Cambridge, Noto, and Darnhall. All observations were performed in phase referenced mode and each source was observed for a total of ∼2 h, split into two

Table 5.2: 2D distribution of the 6.7 GHz CH_3OH maser emission.

Source	$\Delta\alpha$ (mas)	$\Delta\delta$ (mas)	a (mas)	b (mas)	PA (°)
AFGL 5142	+213.3	-440.1	184.2	124.3	-1
G73.06	+528.5	+657.2	342.6	47.2	-78
G78.12	-436.4	-296.6	306.0	43.9	81

Notes: The positional offsets $\Delta\alpha$ and $\Delta\delta$ refer to the positions of Table 5.1, also reported are the major axes (a), minor axes (b) and position angles (PA).

one hour blocks separated by a few hours to improve the uv-coverage. Each one hour block included observation of a strong calibrator at the beginning and end of the block, the remaining observing time was spent switching between the target source and a nearby calibrator (3 min + 2 min). Table 5.1 lists target coordinates and calibrator details. The receivers were set up with the rest frequency of 6668.5142 MHz and a bandwidth of 2 MHz with 1024 channels, corresponding to a velocity resolution of 0.088 km s^{-1} and a total velocity coverage of 90 km s^{-1}. Both right and left circular polarisation were recorded.

The data were correlated on the EVN correlator at JIVE with a short integration time of 0.25 s to facilitate the possibility of performing a wide field search in a larger area surrounding the known maser position. All data reduction and analysis were performed in AIPS following the same recipe as described in Chapter 2. For some sources the phase calibrator was too weak to image directly and for these sources reverse phase referencing was performed. After initial calibration on the brightest maser channel the calibration was applied to the phase reference source and the offset in position measured and applied to the clean maser cube.

The final image cubes have an rms of 2 mJy beam^{-1} in the case of G73.06 and G78.12, and 4 mJy beam^{-1} in the case of AFGL 5142. These cubes were searched for maser spots with the AIPS task SAD. Stepping through the cube on a channel by channel basis all spots with a signal to noise larger than five were fitted by a Gaussian. The list of maser spots was then manually inspected and spurious spots that did not have any adjacent neighbour were removed.

5.3 Results

We have successfully mapped three (AFGL 5142, G73.06, and G78.12) of the five sources with the EVN that have compact thermal methanol emission. Due to the weak flux levels of both target and calibrator sources, we were unable to calibrate and image the two sources G40.62-0.14 and L1206 with these observations. The observations were performed in phase referenced mode and we estimate the absolute position to be accurate to $\sim$ 1 mas (Chapter 2).

In Fig. 5.1 we present the spectra and maser spot distribution of the three sources,

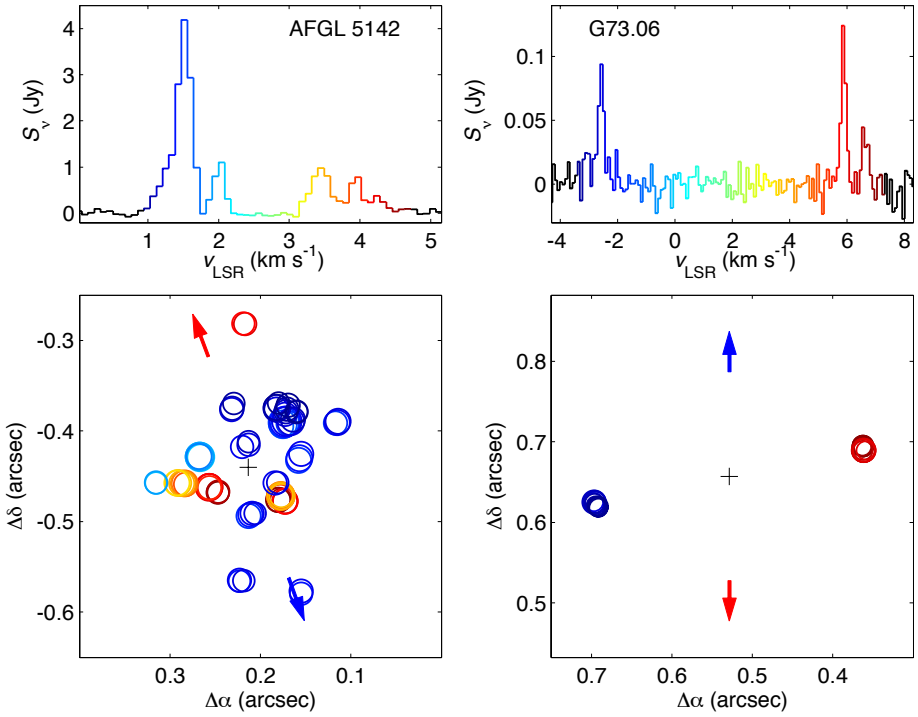

Figure 5.1: Spectrum of the maser emission and maps of the individual spots for the sources AFGL 5142, G73.06, and G78.12. The area of the circles is proportional to the logarithm of the maser flux. The arrows indicate the direction of the thermal CH_3OH outflow (Chapter 4).

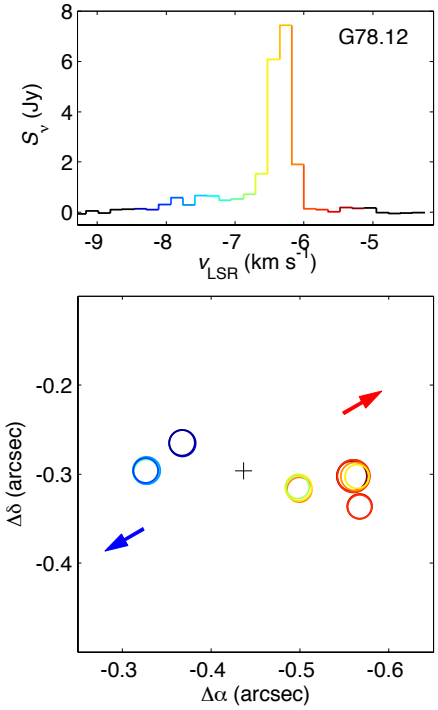

Figure 5.1: continued.

and the individual spots are reported in Table 5.3. Furthermore, we have summarised the maser spot properties by their 2D distribution in Table 5.2. All positions are relative to the absolute positions in Table 5.1. To illustrate the details the of the maser spot distribution we represent all maser spots in each velocity channel by a circle. Spurious single channel spots that do not have any neighbour in any adjacent velocity channel have been excluded. For AFGL 5142 and G73.06 the channel separation is $0.088\,\mathrm{km\,s^{-1}}$whereas for G78.12 a channel separation of $0.176\,\mathrm{km\,s^{-1}}$ was used to improve the signal to noise ratio. The sizes of the circles are proportional to the logarithm of the maser spot intensity and the colours represent the v_{LSR} as indicated in the spectra.

For the source AFGL 5142 we are able to independently confirm the results of Goddi et al. (2007) who mapped this source at the same epoch as us with greater sensitivity (a total integration time of 12 h). The spectrum shows maser emission between $v_{\mathrm{LSR}} = +1$ and $+5\,\mathrm{km\,s^{-1}}$ and the maser distribution is complex with predominately blueshifted emission to the NW and redshifted emission to the SE. The extent of the maser emission is 184.2 mas, corresponding to 330 AU at a kinematic distance of 1.8 kpc (Snell et al. 1988). The CH_3OH maser emission is closely associated with 22 GHz radio continuum emission between two groups of H_2O masers to the NW and SE (Goddi et al. 2007).

The spectrum of G73.06 (IRAS 20062+3550) shows three CH_3OH maser emission features, one at $v_{\mathrm{LSR}} = -2\,\mathrm{km\,s^{-1}}$ and two close to $+6\,\mathrm{km\,s^{-1}}$. The maser spots are grouped in two distinct clumps with the blueshifted clump to the East and the redshifted clump to the West. The clumps are separated by 342.6 mas, corresponding to 1700 AU at a kinematic distance of 4.9 kpc (Molinari et al. 2002). The maser emission is located between the two HCO^+ cores A and B at the edge of the 3.4mm continuum emission observed by Molinari et al. (2002).

The spectrum of G78.12 (IRAS 20126+4104) shows maser emission between $v_{\mathrm{LSR}} = -8.5$ and $-5.5\,\mathrm{km\,s^{-1}}$, with a bright main feature at $-6.3\,\mathrm{km\,s^{-1}}$. The maser spot distribution has an extent of ∼306.0 mas, corresponding to 502 AU at a parallax distance of 1.64 kpc (Moscadelli et al. 2011) and is oriented in the East - West direction. Our results agree with earlier studies of the CH_3OH maser emission in this source (Minier et al. 2001, Edris et al. 2005, Moscadelli et al. 2011) and the maser emission appears to be originating in the NE part of the molecular disk, offset by ∼ 200 mas from the protostar (Cesaroni et al. 2005).

5.4 Discussion

The aim of this work is to test our hypothesis that there is a common origin of the thermal CH_3OH emission reported in Chapter 4 and the CH_3OH maser emission reported in this chapter. In order to establish the orientation of the sources we have also included auxiliary data from the literature where available.

The seven sources studied in this chapter are all characterised by the extent of their thermal CH_3OH distribution being confined to <0.4 pc. We find that for all seven sources the CH_3OH maser position coincides to within 0.05 pc of the centre of the thermal CH_3OH emission. The errors are dominated by the pointing error of the JCMT (∼1″) (Chapter 4)

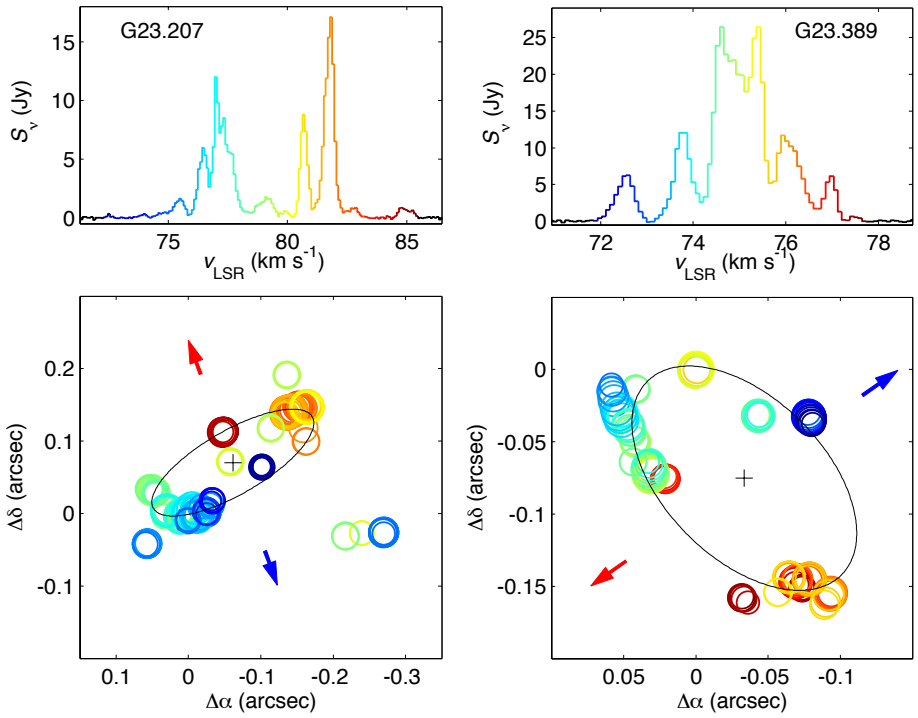

Figure 5.1: Spectrum of the maser emission and maps of the individual spots for the two sources G23.207 and G23.389 (Bartkiewicz et al. 2009). The area of the circles is proportional to the logarithm of the maser flux, also indicated is the elliptical fit of the maser distribution. The arrows indicate the direction of the thermal CH_3OH outflow (Chapter 4).

and the large uncertainty of the (kinematic) distance estimate towards several sources. The maser distributions mapped in this chapter have sizes between 0.18″ and 0.34″ which corresponds to physical sizes between 330 and 1700 AU at the distance of the sources. These are typical extents of methanol masers, although for at least the source G78.12 the masers do not trace the entire circumstellar torus around the protostellar object. Initially we tested a model in which the maser spots were fitted by an ellipse and the velocity field was represented by a rotational and a radial velocity component. However, as argued below, for the three sources mapped with the EVN such an elliptical distribution is not appropriate.

It has also been argued that in at least some sources the long baselines of VLBI filter out larger scale source structure and that observations with shorter baselines are needed to recover these larger structures (Pandian et al. 2011). While we cannot show conclusively that this is not the case for the sources we have observed, we compare the VLBI spectra to those of single dish observations in the literature. The single dish observations are observed at different epochs to the VLBI observations and due to the variability of the maser emission we can only compare the general shape of the different components and the velocity span of the emission. The two sources AFGL 5142 and G78.12 (and Cep A HW2) have been observed with the Effelsberg telescope by Vlemmings (2008) and although only a fraction (10%) of the total flux is recovered in the VLBI observations, the spectra are qualitatively very similar. Likewise, the observations of Szymczak et al. (2000) with the Toruń telescope reveal that the spectra of G73.06, G23.207 and G23.389 is qualitatively very similar to the VLBI spectra of these sources with a wide range of recovered fluxes. The affinity of the VLBI spectra and the single dish spectra suggests that the VLBI maps represents the whole maser structure. The missing flux filtered out by the long VLBI baselines may arise in a more extended halo around the compact maser spots seen in the VLBI maps.

The two sources G23.207 and G23.389 have an elliptical distribution of CH_3OH masers (Bartkiewicz et al. 2009), and the major axes of the CH_3OH maser is roughly perpendicular to the velocity gradient seen in thermal methanol emission, Fig. 5.1. We interpret the thermal CH_3OH velocity gradient as an indicator of the early stages of a molecular outflow and use it to constrain the orientation of these sources. Bartkiewicz et al. (2009) fitted ellipses to the maser positions and used the velocity field of the maser spots to test a model with a radial and a rotational velocity component. However, without further constraints it is not possible to determine the sign of the velocity components. With the velocity gradient from our thermal CH_3OH observations in mind we interpret the near side of the ring to be to the NE in the case of G23.207 and to the SE in the case of G23.389. For both sources the radial velocity component found by Bartkiewicz et al. (2009) is then that of infall, similar to what was seen in Cepheus A HW2 (Chapter 2).

The remaining five sources do not show any elliptical maser distribution that can easily be used to determine the orientation and we therefore need to discuss them in some detail. Most of the sources are well studied and the recent literature can be used to determine the orientation of outflows and in some cases disks. Below we argue that in general the orientation of the thermal CH_3OH emission is in agreement with outflows seen in other molecular species and that in several cases the CH_3OH maser distribution appears to be

perpendicular to the outflows.

In the source G78.12 (IRAS 20126+4104) the methanol masers are associated with an YSO of ∼7 $M_\odot$ still in its accreting phase, with a molecular disk with a position angle of 53° and an outflow roughly perpendicular to the disk (PA=−60°) (Cesaroni et al. 2005). Supporting this are the multi-epoch H_2O maser observations of Moscadelli et al. (2011) who find the water masers to trace a conical jet with a position angle of −65°, in good agreement with the molecular outflow. Our thermal CH_3OH observations show a clear velocity gradient with a similar position angle (∼−60°). The velocities and proper motions of the CH_3OH maser spots suggest that the CH_3OH masers are located in two distinct groups, the westernmost that seem to be associated with a disk/outflow interface and the easternmost that are lying in the plane of the disk (Moscadelli et al. 2011). Disregarding the second group associated with the outflow interface the methanol maser distribution is roughly perpendicular to the outflow, though they only trace a very small segment of the disk (Fig. 5.1c).

AFGL 5142 is a complex cluster with five millimetre continuum cores (MM-1–5) within 5″ and at least three different molecular outflows (A–C) with position angles of 5°, 35°, and −60° (Zhang et al. 2007). Both H_2O and CH_3OH masers are associated with MM-1 (Hunter et al. 1999, Goddi & Moscadelli 2006, Goddi et al. 2007). The H_2O masers trace a bipolar outflow with a position angle of −40°and it is therefore thought that outflow C is associated with MM-1 (Zhang et al. 2007). Furthermore, the core MM-1 is associated with radio continuum emission at 3.6, 8.4, and 22 GHz (Goddi & Moscadelli 2006, Zhang et al. 2007). The 3.6 GHz emission is double peaked, possibly tracing a jet with a position angle of −29°. In contrast, the higher frequency centimetre emission is single peaked and centred between the two groups of H_2O masers. The CH_3OH masers are situated between the two groups of H_2O masers, close to the centre of the high frequency centimetre continuum peak. Goddi et al. (2007) proposed that while the H_2O masers trace the two outflow cones, the velocity field of the CH_3OH masers is better described by a radial infall model. Our CH_3OH maser results agree with this interpretation, although we cannot extend the analysis as the observations were performed at the same epoch. The thermal CH_3OH observations in Chapter 4 show a velocity gradient with a position angle of 20° which is in agreement with the findings of Zhang et al. (2007). It does however suggest that MM-1 may not be the major driving source of the thermal CH_3OH in the region, though they observe that there seems to be some contribution to the thermal CH_3OH from outflow "C" (Fig. 5.1a). Clearly, the lower-resolution JCMT thermal CH_3OH observations cannot be used to determine the outflow direction of the YSO associated with the maser emission and further high-resolution observations are needed to disentangle the dynamics of this cluster.

In G73.06 Molinari et al. (2002) observed a complex velocity field with four HCO^+ cores (A–D) of which core B has a 3.4 mm counterpart. The CH_3OH maser emission occurs between core A and B, on the edge of the millimetre continuum emission. The line wings of the HCO^+ emission indicate blueshifted emission to the North and redshifted emission to the South, in agreement with the velocity field seen in CO (Zhang et al. 2005). Varricatt et al. (2010) observed an outflow with position angles 43° and 212° in H_2 (2.12 μm) emission and pinned the driving source of the outflow to within 0.5″

of the CH_3OH maser position. It is difficult to determine any preferred direction from the thermal CH_3OH map (Chapter 4) but we note that the centre of the thermal CH_3OH ellipsoid agrees well with the maser position and the outflows seen in other tracers are perpendicular to the methanol maser distribution (Fig. 5.1b).

The two sources L1206 and G40.62 for which we were unable to map the CH_3OH maser emission have previously been studied with interferometers. Voronkov & Slysh (2002) observed L1206 with the EVN and found the CH_3OH maser emission in two clumps ("A" and "B") separated by 200 mas and with a position angle of $-65°$. They argue that feature "A" may trace a disk in roughly N-S direction which would place feature "B" in the outflow. However, such velocity gradients as seen in feature "A" have been observed in many maser clumps and may be due to the nature of the maser emission and should not necessarily be interpreted as a disk signature. Nevertheless, the position of the CH_3OH maser emission is close to the centre of the centroid fitted to the thermal CH_3OH emission in Chapter 4, though it is difficult to interpret the velocity field.

G40.62 was observed with the ATCA by Beuther et al. (2002) and found to have only a single CH_3OH maser clump associated with millimetre dust continuum, H_2O masers, centimetre continuum emission, and a MIR source. The position of the CH_3OH maser is close to the centre of the ellipsoid of the thermal CH_3OH emission that has a velocity gradient in the SE-NW direction.

A further complication when comparing the AU size CH_3OH maser distribution to that of the parsec size thermal CH_3OH is the size scales on which they occur and the dynamical processes that occur. Precessing jets have been inferred in several high-mass star-forming sources (e.g., Cep A HW2 and G78.12) and it can therefore be difficult to trace the larger scale outflow back to the YSO and infer the orientation of the disk/outflow system (Cunningham et al. 2009, Cesaroni et al. 2005). To make clear the link between the CH_3OH maser emission and the thermal CH_3OH emission higher resolution studies of the thermal gas are in order.

5.5 Summary

We have mapped the 6.7 GHz CH_3OH emission in three high-mass star-forming regions. We have also included the results of four more sources from the literature for comparison with the thermal CH_3OH results in Chapter 4.

In the three CH_3OH maser sources that we have mapped, the maser emission extends over 330 – 1700 AU, similar to what has been found in other high-resolution studies of masers and in agreement with the four extra sources included in this chapter. The velocity field of the masers cover $\sim 3 - 4\,\mathrm{km\,s^{-1}}$, also in agreement with what is typically found for CH_3OH maser emission.

A comparison of the VLBI spectra to single dish spectra from the literature show that although the VLBI spectra only recover a fraction of the single dish flux, in all sources, most of the components seen in the single dish spectra are present in the VLBI spectra and span a similar velocity range. This suggest that although the maser spots seen with VLBI are embedded in more extended maser emission the compact emission represents

the whole physical structure, consistent with the core/halo pattern observed by Minier et al. (2002).

The CH_3OH maser emission in all seven sources arises close to the centre (<0.05 pc) of the thermal CH_3OH emission, consistent with a single common origin of the gas phase CH_3OH gas, as was found for Cep A HW2 in Chapter 2. Furthermore, in at least three of the seven sources discussed in this chapter the maser emission seem to delineate or be part of a disk with a major axis orthogonal to a velocity gradient seen in the larger scale thermal CH_3OH emission. In some sources the velocity gradient is parallel to known molecular outflows and we suggest that the thermal CH_3OH gas is entrained in a bipolar outflow.

To probe the masing gas on size scales similar to the CH_3OH maser emission and further investigate the link between the arc second scale maser emission and the larger scale ($10''$– $20''$) thermal CH_3OH emission high resolution studies are required. With the advent of ALMA such high resolution studies of larger samples will now be possible. In conjunction with high-sensitivity high-resolution studies of the radio continuum emission with instruments such as the EVLA and improved distance estimates to these objects the physical processes at play can be quantified much better.

Acknowledgements

This research was supported by the EU Framework 6 Marie Curie Early Stage Training programme under contract number MEST-CT-2005-19669 “ESTRELA”.

Table 5.3: Measured maser spots in the three sources mapped.

v_{LSR} (km s^{-1})	$\Delta\alpha$ (mas)	$\Delta\delta$ (mas)	S_{p} (mJy beam^{-1})
AFGL 5142			
4.371	180.5	-476.3	103
4.371	246.7	-468.0	45
4.283	179.9	-475.9	112
4.283	247.0	-468.0	63
4.195	246.4	-466.9	61
4.195	177.0	-475.6	42
4.107	256.1	-461.9	253
4.107	172.6	-477.7	94
4.019	256.5	-462.2	349
4.019	172.8	-477.4	166
4.019	216.6	-281.9	56
3.932	256.5	-461.9	241
3.932	172.7	-477.4	145
3.932	218.8	-281.6	50
3.844	256.1	-462.6	75
3.756	178.0	-472.3	69
3.668	177.8	-472.0	187
3.668	282.8	-458.6	87
3.580	177.5	-471.6	379
3.580	283.6	-457.9	185
3.493	177.3	-471.6	443
3.493	284.9	-457.9	149
3.405	177.1	-471.6	304
3.405	287.1	-457.9	138
3.317	290.5	-457.6	180
3.317	176.8	-471.2	91
3.229	292.2	-457.2	154
2.176	266.2	-429.1	197
2.088	266.7	-428.8	532
2.088	315.3	-457.2	44
2.000	267.4	-428.4	466
2.000	315.4	-456.8	53
1.912	267.9	-428.4	160
1.824	176.0	-394.9	58
1.737	175.1	-392.8	445
1.649	174.0	-391.0	1209
1.649	157.8	-432.4	163
1.649	168.7	-391.7	106

Table 5.3: Continued.

$v_{\rm LSR}$ (km s^{-1})	$\Delta\alpha$ (mas)	$\Delta\delta$ (mas)	$S_{\rm p}$ (mJy beam^{-1})
1.649	213.2	-493.9	96
AFGL 5142			
1.649	116.9	-391.3	72
1.561	172.4	-389.9	1531
1.561	156.8	-430.2	241
1.561	210.9	-492.5	110
1.561	155.0	-580.0	51
1.561	222.9	-565.9	49
1.473	170.5	-389.5	907
1.473	114.8	-391.0	161
1.473	155.1	-425.2	117
1.473	183.8	-457.6	78
1.473	209.3	-491.0	75
1.473	222.9	-564.8	74
1.473	154.8	-577.1	69
1.473	220.4	-417.6	56
1.385	166.2	-389.9	360
1.385	114.0	-389.5	149
1.385	182.2	-376.6	93
1.385	231.6	-376.6	86
1.385	172.7	-381.6	79
1.385	212.9	-415.1	58
1.385	205.8	-491.0	47
1.385	181.0	-456.8	45
1.385	218.2	-565.2	45
1.298	181.9	-375.1	269
1.298	164.0	-387.4	119
1.298	231.0	-374.8	90
1.298	171.5	-378.7	73
1.298	213.1	-411.8	43
1.210	182.2	-374.0	171
1.210	170.9	-375.8	73
1.210	160.0	-379.1	50
1.210	229.3	-369.7	45
1.122	169.3	-371.5	74
1.122	159.6	-378.4	43
1.122	179.8	-369.0	41
G73.06			
6.780	362.9	694.4	25
6.692	362.5	694.4	35

Table 5.3: Continued.

v_{LSR} (km s^{-1})	$\Delta\alpha$ (mas)	$\Delta\delta$ (mas)	S_{p} (mJy beam^{-1})
6.604	362.5	694.4	33
6.517	362.5	693.4	20
6.429	362.9	693.7	10
6.078	362.2	689.4	18
5.990	361.8	689.4	87
5.902	361.1	689.4	80
5.814	360.7	689.0	51
5.726	359.1	689.0	15
-2.351	696.6	625.3	13
-2.439	696.2	625.0	53
-2.527	696.6	625.0	79
-2.615	695.9	624.6	45
-2.702	696.2	623.5	19
-2.790	695.2	621.4	12
-2.878	694.1	620.3	13
-2.966	692.3	619.2	14
-3.054	691.9	619.6	24
-3.141	691.2	618.1	15
G78.12			
-6.000	-558.7	-301.9	1454
-6.176	-559.8	-301.9	5827
-6.176	-567.0	-336.4	146
-6.351	-560.5	-302.3	4689
-6.351	-567.4	-336.5	114
-6.527	-562.0	-302.5	778
-6.527	-499.7	-317.3	152
-6.702	-498.6	-315.3	254
-6.702	-564.5	-302.4	110
-6.878	-497.5	-314.4	81
-7.054	-327.1	-297.5	170
-7.229	-327.5	-296.4	352
-7.405	-327.5	-296.0	477
-7.580	-326.8	-296.0	170
-7.756	-367.9	-265.4	266
-7.932	-367.6	-265.0	207